JASA LETTER TO THE EDITOR

A non-paraxial model for the audio sound behind a non-baffled parametric array loudspeaker (L)

Jiaxin Zhong,[a] Ray Kirby,[b] and Xiaojun Qiu[c]
Centre for Audio, Acoustics and Vibration, Faculty of Engineering and Information Technology, University of Technology Sydney, Sydney, New South Wales 2007, Australia

ABSTRACT:
It has been reported that audible sounds can be heard behind a parametric array loudspeaker in free field, which cannot be predicted by existing models. A non-paraxial model is developed in this paper for the finite size and disk-shaped parametric source based on quasilinear approximation and disk scattering theory. The sounds on both front and back sides are calculated numerically and compared with the existing non-paraxial model for the parametric source installed in an infinitely large baffle. Both simulation and experiment results show that audible sound exists on the back side. The mechanism of the phenomenon is explored. © *2020 Acoustical Society of America*.
https://doi.org/10.1121/10.0000793
(Received 22 October 2019; revised 16 January 2020; accepted 6 February 2020; published online 6 March 2020)
[Editor: Mark Hamilton] Pages: 1577–1580

I. INTRODUCTION

The parametric array loudspeaker (PAL) is an application of parametric acoustic arrays for radiating highly directional audio sounds in air where the carrier wave is ultrasound.[1] The most accurate existing theoretical models of PALs assume that a PAL is placed on an infinitely large baffle, which means that no sounds propagate to the back side of the PAL.[2] However, audible sounds on the back side of a PAL were detected in PAL applications because audio sounds can diffract to the back side.[3] An analytical model for non-baffled PALs will be developed in this paper for predicting the sound field on the back side of a finite size PAL.

When a PAL radiates two intensive ultrasound (primary) waves at different frequencies, secondary waves which contain the difference-frequency wave (the audio sound in air) are generated due to nonlinearity. The most widely used model for predicting audio sound is the Khokhlov-Zabolotskaya-Kuznetsov (KZK) equation but the results are usually only valid in front of the PAL and inside the paraxial region about 20° from the transducer axis.[4] A non-paraxial model with better accuracy for baffled PALs was proposed.[2] By applying the Gaussian beam expansion method to ultrasounds, the computation of audio sounds is reduced to a three-fold integral which can be used to predict near-field and wide-angle far-field sound fields. However, all of the aforementioned models cannot be used to predict the sound behind a non-baffled PAL.

PALs are usually manufactured in circular or square shapes with small thickness, so it can be treated as a finite size disk or square plate. The sound scattering by a finite size disk can be solved analytically,[5] so the disk-shaped PAL is considered in this paper. The solution consists of the spheroidal wave functions derived from the oblate spheroidal coordinate system.[6,7] In this paper, each virtual audio source generated by ultrasounds of a PAL in space is regarded as a point monopole so that its scattered sound by the finite size disk can be solved.

II. THEORY

The sketch of the model is shown in Fig. 1. A circular PAL with a radius of a in free field generates two harmonic ultrasounds with frequencies f_1 and f_2 ($f_1 > f_2$) with the boundary condition on the transducer surface being

$$v_z(x,y,t) = v_1(x,y)\mathrm{e}^{-\mathrm{j}\omega_1 t} + v_2(x,y)\mathrm{e}^{-\mathrm{j}\omega_2 t}, \tag{1}$$

where j is the complex unit, v_z represents the vibration velocity normal to the transducer surface, v_i is the amplitude of the vibration velocity, $i = 1, 2$, $\omega_i = 2\pi f_i$ is the angular frequency of the ith primary wave, (x, y) is the transverse coordinate, and the axis z is normal to the transducer surface under the coordinate system O-xyz. The solutions of the ultrasounds and audio sound with the frequency $f_\mathrm{a} = f_1 - f_2$ are denoted as

$$\tilde{p}_i(\mathbf{r},t) = p_i(\mathbf{r})\mathrm{e}^{-\mathrm{j}\omega_i t},\ i = 1, 2, \mathrm{a}, \tag{2}$$

where the subscript "1," "2," and "a" represent the two ultrasounds and the audio sound respectively, and $\mathbf{r} = (x, y, z)$ is a field location.

Because the ultrasound level generated by a PAL is limited due to safety concerns, the nonlinearity is not very strong and the quasilinear approximation can be used in the

[a]Electronic mail: Jiaxin.Zhong@student.uts.edu.au, ORCID: 0000-0002-9972-8004
[b]ORCID: 0000-0002-3520-1377
[c]ORCID: 0000-0002-5181-1220

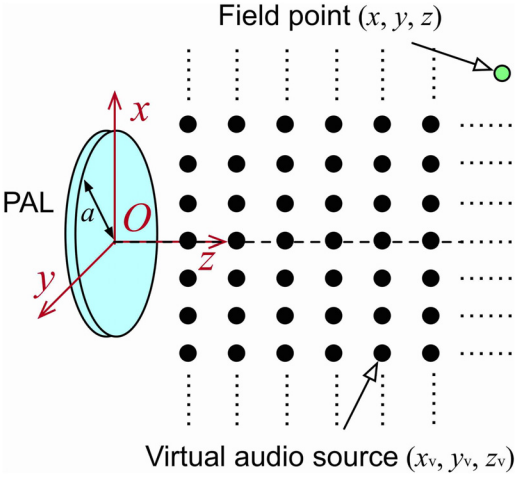

FIG. 1. (Color online) The sketch of the model.

derivation.[1] With the successive method, the sound pressure of the ultrasounds can be expressed by Rayleigh integral as[2]

$$p_i(\mathbf{r}) = -2\mathrm{j}\rho_0\omega_i \int_{-\infty}^{\infty}\int_{-\infty}^{\infty} v_i(x_\mathrm{s}, y_\mathrm{s}) \frac{\mathrm{e}^{\mathrm{j}k_i d_\mathrm{s}}}{4\pi d_\mathrm{s}} \mathrm{d}x_\mathrm{s}\mathrm{d}y_\mathrm{s}, \tag{3}$$

where $k_i = \omega_i/c_0 + \mathrm{j}\alpha_i$, α_i is the sound attenuation coefficient at the frequency f_i,[8] $i = 1$ and 2, and $d_\mathrm{s} = \sqrt{(x - x_\mathrm{s})^2 + (y - y_\mathrm{s})^2 + z^2}$ is the distance between the field point $\mathbf{r}$ and the source point $(x_\mathrm{s}, y_\mathrm{s}, 0)$ on the transducer surface.

If the PAL is placed on an infinitely large baffle, the audio sound can be treated as the superposition of the sounds generated by infinitely many virtual sources at $\mathbf{r}_\mathrm{v} = (x_\mathrm{v}, y_\mathrm{v}, z_\mathrm{v})$ and their image sources at $(x_\mathrm{v}, y_\mathrm{v}, -z_\mathrm{v})$ which has the source density function of

$$q(\mathbf{r}_\mathrm{v}) = -\frac{\mathrm{j}\beta\omega_\mathrm{a}}{\rho_0^2 c_0^4} p_1(\mathbf{r}_\mathrm{v}) p_2^*(\mathbf{r}_\mathrm{v}), \quad z_\mathrm{v} > 0. \tag{4}$$

The audio sound near an infinitely large baffle is then expressed as[2] (denoted by "baffled model")

$$p_\mathrm{a}(\mathbf{r}) = -\mathrm{j}\rho_0\omega_\mathrm{a} \int_0^{\infty}\int_{-\infty}^{\infty}\int_{-\infty}^{\infty} q(\mathbf{r}_\mathrm{v}) \times \left(\frac{\mathrm{e}^{\mathrm{j}k_\mathrm{a}d_{\mathrm{v},+}}}{4\pi d_{\mathrm{v},+}} + \frac{\mathrm{e}^{\mathrm{j}k_\mathrm{a}d_{\mathrm{v},-}}}{4\pi d_{\mathrm{v},-}}\right) \mathrm{d}x_\mathrm{v}\mathrm{d}y_\mathrm{v}\mathrm{d}z_\mathrm{v}, \quad z > 0, \tag{5}$$

where $k_\mathrm{a} = \omega_\mathrm{a}/c_0 + \mathrm{j}\alpha_\mathrm{a}$, α_a is the sound attenuation coefficient at the frequency f_a, and $d_{\mathrm{v},\pm} = \sqrt{(x - x_\mathrm{v})^2 + (y - y_\mathrm{v})^2 + (z \mp z_\mathrm{v})^2}$ is the distance between the field point $\mathbf{r}$ and the virtual source $(d_{\mathrm{v},+})$ or its image source $(d_{\mathrm{v},-})$.

Although the sound pressure of ultrasounds can be expressed as Eq. (3) for non-baffled PALs due to the fact that the size of PALs is usually large enough compared with the wavelength of ultrasounds, the PALs usually cannot be considered as infinitely large for the audio sounds. Each virtual audio source with the source density function shown in Eq. (4) is scattered by the disk. The boundary of the disk is assumed to be rigid for audio sounds, so it has[9]

$$\left.\frac{\partial p_\mathrm{a}}{\partial \xi}\right|_{\xi=\xi_\mathrm{b}=0} = 0, \tag{6}$$

where ξ is the radial oblate spheroidal coordinate in the oblate spheroidal coordinate system, ξ_b represents the coordinate of the boundary surface.[9]

When the radial coordinate $\xi = \xi_\mathrm{b} = 0$, the oblate represents an infinitely thin disk with a radius of a centered at O on the plane xOy. The total sound pressure at a field point $\mathbf{r}$ radiated by a non-baffled disk-shaped PAL is the superposition of the direct and scattered sounds generated by virtual audio sources (denoted by "non-baffled model")

$$p_{\mathrm{a,t}}(\mathbf{r}) = -\mathrm{j}\rho_0\omega_\mathrm{a}a^3 \int_0^{2\pi}\int_0^{1}\int_0^{\infty} q(\mathbf{r}_\mathrm{v}) G(\mathbf{r}, \mathbf{r}_\mathrm{v}) \times (\xi_\mathrm{v}^2 + \eta_\mathrm{v}^2)\mathrm{d}\xi_\mathrm{v}\mathrm{d}\eta_\mathrm{v}\mathrm{d}\varphi_\mathrm{v}, \quad z < 0 \,\mathrm{or}\, z > 0, \tag{7}$$

where the relation $\mathrm{d}x_\mathrm{v}\mathrm{d}y_\mathrm{v}\mathrm{d}z_\mathrm{v} = a^3(\xi_\mathrm{v}^2 + \eta_\mathrm{v}^2)\mathrm{d}\xi_\mathrm{v}\mathrm{d}\eta_\mathrm{v}\mathrm{d}\varphi_\mathrm{v}$ is used. $G(\mathbf{r}, \mathbf{r}_\mathrm{v})$ is the Green function in the presence of a rigid disk and can be expressed as[9]

$$G(\mathbf{r}, \mathbf{r}_\mathrm{v}) = \frac{\mathrm{j}k_\mathrm{a}}{2\pi}\sum_{m=0}^{\infty}\sum_{n=m}^{\infty} \varepsilon_m \chi_{mn}(-\mathrm{j}k_\mathrm{a}a, \mathrm{j}\xi, \mathrm{j}\xi_\mathrm{v}) \times S_{mn}(-\mathrm{j}k_\mathrm{a}a, \eta) S_{mn}(-\mathrm{j}k_\mathrm{a}a, \eta_\mathrm{v}) \times \cos\left[m(\varphi - \varphi_\mathrm{v})\right], \tag{8}$$

$$\chi_{mn}(-\mathrm{j}k_\mathrm{a}a, \mathrm{j}\xi, \mathrm{j}\xi_\mathrm{v}) = R_{mn}^{(1)}(-\mathrm{j}k_\mathrm{a}a, \mathrm{j}\xi_<) R_{mn}^{(3)}(-\mathrm{j}k_\mathrm{a}a, \mathrm{j}\xi_>) - \frac{R_{mn}^{(1)\prime}(-\mathrm{j}k_\mathrm{a}a, \mathrm{j}\xi_\mathrm{b})}{R_{mn}^{(3)\prime}(-\mathrm{j}k_\mathrm{a}a, \mathrm{j}\xi_\mathrm{b})} R_{mn}^{(3)}(-\mathrm{j}k_\mathrm{a}a, \mathrm{j}\xi) \times R_{mn}^{(3)}(-\mathrm{j}k_\mathrm{a}a, \mathrm{j}\xi_\mathrm{v}), \tag{9}$$

where $\mathbf{r}_\mathrm{v} = (\eta_\mathrm{v}, \xi_\mathrm{v}, \varphi_\mathrm{v})$ is the location of the virtual audio source in the oblate spheroidal coordinate system, i.e., $\varepsilon_m = 1$ for $m = 0$ and $\varepsilon_m = 2$ for $m \neq 0$, $\xi_> = \max(\xi, \xi_\mathrm{v})$, and $\xi_< = \min(\xi, \xi_\mathrm{v})$. $S_{mn}(-\mathrm{j}k_\mathrm{a}a, \eta)$ is the normalized angular oblate spheroidal wave function, $R_{mn}^{(i)}(-\mathrm{j}k_\mathrm{a}a, \mathrm{j}\xi)$ and $R_{mn}^{(i)\prime}(-\mathrm{j}k_\mathrm{a}a, \mathrm{j}\xi)$ are the ith kind of the radial oblate spheroidal wave functions and their derivatives with respect to ξ, respectively, $i = 1$, 3. The readers may refer to Refs. 6 and 7 for the computations of these special functions.

When the surface of the transducer is axisymmetric about its axis, the source density function of audio virtual sources is axisymmetric, so the total audio sound of the non-baffled model Eq. (7) can be simplified by integrating the azimuthal angle φ_v, yielding

$$p_{\mathrm{a,t}}(\mathbf{r}) = -2\mathrm{j}\pi\rho_0\omega_\mathrm{a}a^3 \int_0^{1}\int_0^{\infty} q(\mathbf{r}_\mathrm{v}) G_0(\mathbf{r}, \mathbf{r}_\mathrm{v}) \times (\xi_\mathrm{v}^2 + \eta_\mathrm{v}^2)\mathrm{d}\xi_\mathrm{v}\mathrm{d}\eta_\mathrm{v}, \quad z < 0 \,\mathrm{or}\, z > 0, \tag{10}$$

https://doi.org/10.1121/10.0000793

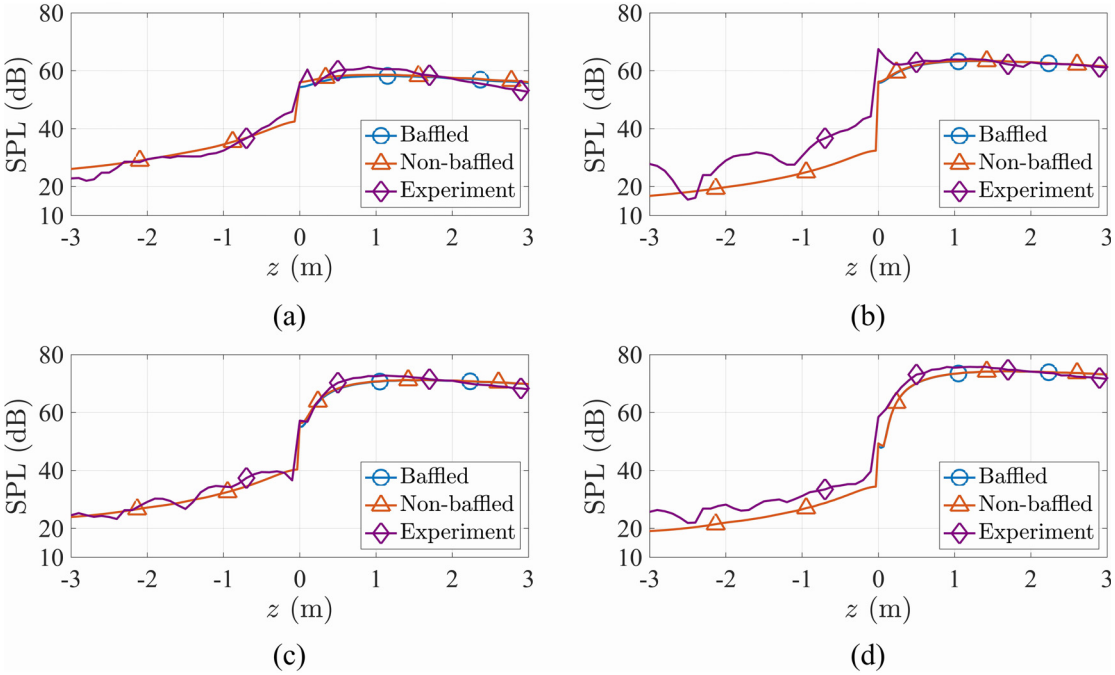

FIG. 2. (Color online) SPLs along the z axis at different audio frequencies: (a) 315 Hz, (b) 500 Hz, (c) 800 Hz, and (d) 1 kHz.

$$G_0(\mathbf{r},\mathbf{r}_v) = \frac{jk_a}{2\pi}\sum_{n=0}^{\infty}\chi_{0n}(-jk_a a, j\xi, j\xi_v) \times S_{0n}(-jk_a a,\eta)S_{0n}(-jk_a a,\eta_v). \quad (11)$$

III. RESULTS AND DISCUSSIONS

The experiments were conducted in the hemi-anechoic room with dimensions of 7.20 m × 5.19 × 6.77 m (height) and the PAL is a Holosonics Audio Spotlight AS-24i with the size of 0.6 m × 0.6 m. In simulations, a circular piston was driven with a uniform surface vibration velocity amplitude and the radius was set as 0.3385 m so that its area is the same as that of the rectangular PAL used in experiments, i.e., $0.6^2 \approx \pi \times 0.3385^2$. The relative humidity and the temperature were 60% and 25 °C, respectively. The carrier frequency of the PAL is 64 kHz. The air attenuation coefficient are calculated according to ISO 9613-1.[10]

The sound field was measured at a rectangular grid with $60 \times 61 = 3661$ points in the yOz plane at the height of 1.8 m. 60 microphones were located in the y direction from $y = -1.45$ m to $y = 1.5$ m with a spacing of 5 cm and they were measured simultaneously with a custom made 60-channel microphone array. The microphone array was located at 61 different positions in the z direction from $z = -3$ m to $z = 3$ m with a spacing of 10 cm. All the measurement microphones are Brüel & Kjær type 4957. To avoid the spurious sounds at microphones induced by the intensive ultrasounds radiated by the PAL, all the microphones are covered by a piece of small and thin plastic film.[11]

Figure 2 shows sound pressure levels (SPLs) of audio sounds along the z axis generated by the finite size disk-shaped PAL using the baffled and non-baffled models and the experimental results. All SPLs in the simulations are normalized to a value so that the SPL at $z = 2.0$ m for the baffled PAL is the same as that measured in the experiments. It can be found that the values from both models at all frequencies are almost the same at locations far away in front of the PAL. The experimental results on both front and back sides of the PAL are generally in accordance with those predicated by the non-baffled model. Large errors occur at 500 Hz when $z < 0.2$ m which might be caused by the measurement errors, the reflection of grounds, the shape of the PAL, and the scattering effects of the equipment.

The curves of SPL for the non-baffled PAL at $z = -0.1$, -0.25, -0.5, -1.0, and -2.0 m at different frequencies are shown in Fig. 3. The surface SPL of ultrasounds, i.e., the

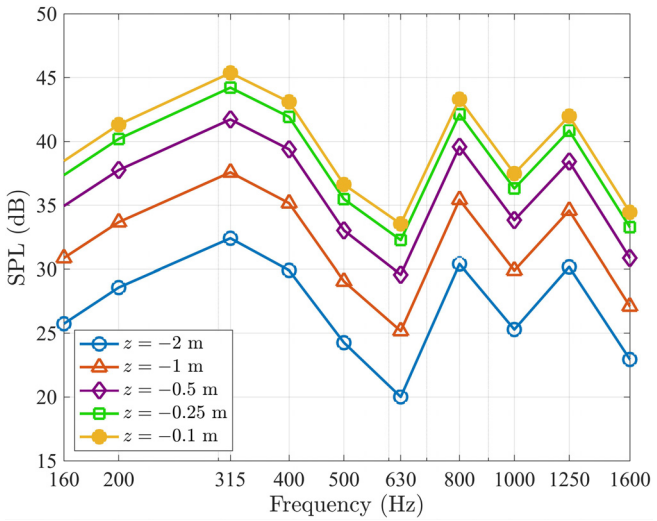

FIG. 3. (Color online) SPLs along the z axis computed with the non-baffled model at 1/3-ocatve center frequencies.

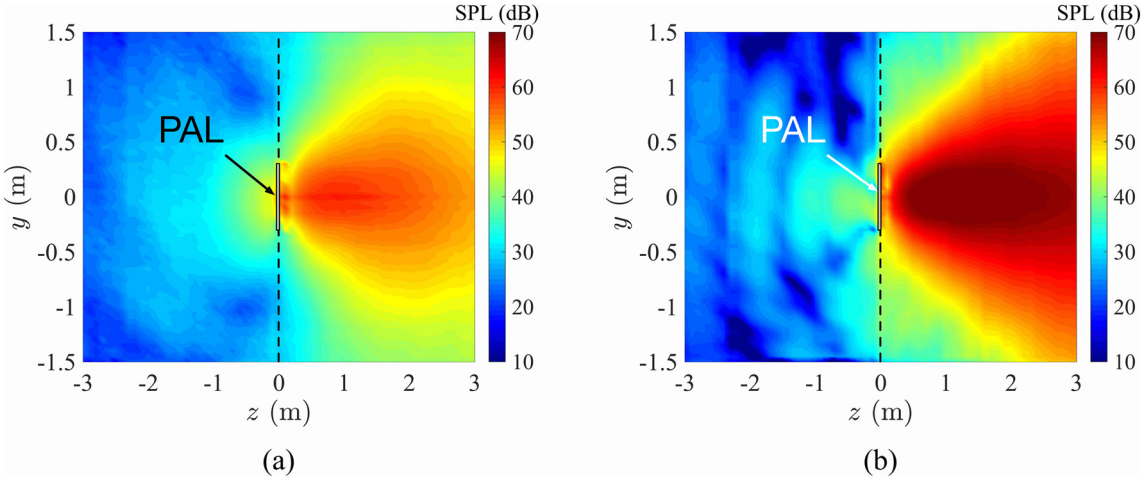

FIG. 4. (Color online) The measured SPLs of audio sounds at (a) 315 Hz and (b) 800 Hz.

level of $\rho_0 c_0 |v_i|$, $i = 1, 2$, is set as 125 dB at all curves. Both Figs. 2 and 3 demonstrate that there are audible sounds on the back side of the PAL which is caused by the diffracting of the finite size disk. For example, the SPL is 45 dB at $z = -0.1$ m at 315 Hz while the audio sound at $z = 1.0$ m in front of the PAL is about 61.4 dB.

The SPL is largest at 315 Hz (the wavelength is 1.09 m) for all cases because the constructive interference of waves is largest when the radius of the PAL is approximately 0.35 times of the wavelength.[9] As the frequency decreases from 315 Hz, the SPL on the back side decreases due to the fact that the frequency response of the PAL decreases significantly (12 dB) as the audio frequency is halved. As the frequency increases from 315 Hz, the SPL on the back side decreases first and then reaches the local maxima at 800 and 1250 Hz because the diffraction effects are weakened first as the wavelength becomes smaller until it reaches other resonant frequencies where the constructive interference of waves is significant.

The SPL distribution in yOz plane at 315 and 800 Hz are shown in Fig. 4. It is found that the audio sounds are audible over a large area on the back side of the PAL. For example, at 315 Hz, there is an approximately circular region centered at the PAL with the radius of about 1.3 m where the SPLs are more than 35 dB. Therefore, the effects of the finite size of the PAL should be taken into account.

IV. CONCLUSIONS

A non-paraxial model for the radiation of a non-baffled parametric array loudspeaker in free field is developed based on quasilinear approximation and disk scattering theory. In this model, each virtual audio source generated by the ultrasounds in space is regarded as a point monopole and its scattered sound by a finite size disk is computed. Both simulation and experiment results demonstrate that audible sound exists on the back side of the PAL, indicating that the effects of the finite size of the PAL should be taken into account.

ACKNOWLEDGMENTS

This research was supported under the Australian Research Council's Linkage Project (Grant No. LP160100616).

[1]W. S. Gan, J. Yang, and T. Kamakura, "A review of parametric acoustic array in air," Appl. Acoust. **73**(12), 1211–1219 (2012).
[2]M. Červenka and M. Bednarik, "Non-paraxial model for a parametric acoustic array," J. Acoust. Soc. Am. **134**(2), 933–938 (2013).
[3]A. Sugahara, H. Lee, S. Sakamoto, and S. Takeoka, "A study on the measurements of the absorption coefficient by using a parametric loudspeaker," in *INTER-NOISE and NOISE-CON Congress and Conference Proceedings*, Hongkong, China (2017), Vol. 255, Issue 4, pp. 3743–3751.
[4]M. F. Hamilton and D. T. Blackstock, *Nonlinear Acoustics* (Acoustical Society of America, New York, 2008).
[5]C. Flammer, *Spheroidal Wave Functions* (Dover Publications, Mineola, NY, 2014).
[6]S. Zhang and J. Jin, *Computation of Special Functions* (Wiley, New York, 1996).
[7]A. L. Van Buren, "Accurate calculation of oblate spheroidal wave functions," arXiv:1708.07929 (2017).
[8]H. E. Bass, L. C. Sutherland, A. J. Zuckerwar, D. T. Blackstock, and D. Hester, "Atmospheric absorption of sound: Further developments," J. Acoust. Soc. Am. **97**(1), 680–683 (1995).
[9]J. Zhong, J. Tao, F. Niu, and X. Qiu, "Effects of a finite size reflecting disk in sound power measurements," Appl. Acoust. **140**(1), 24–29 (2018).
[10]ISO 9613-1:1993: *Acoustics—Attenuation of Sound During Propagation Outdoors—Part 1: Calculation of the Absorption of Sound by the Atmosphere* (International Organization for Standardization, Geneva, 1993).
[11]P. Ji and J. Yang, "An experimental investigation about parameters' effects on spurious sound in parametric loudspeaker," Appl. Acoust. **148**, 67–74 (2019).